High Oxygen Pressures and the Stabilization of the Highest Oxidation States of Transition Metals – Mössbauer Spectroscopic Characterization of the Induced Electronic Phenomena

Gérard Demazeau[a], Alexey Baranov[a,b], Igor Presniakov[b], and Alexey Sobolev[b]

[a] University Bordeaux 1 "Sciences and Technologies", Centre de Ressources Hautes Pressions ICMCB-ENSCPB, 87 Avenue du Dr A. Schweitzer, 33608 Pessac Cedex, France
[b] Department of Chemistry, Lomonosov Moscow State University, 119992 Leninskie Gory, Moscow-V-234, Russia

Reprint requests to Prof. G. Demazeau. E-mail: demazeau@icmcb-bordeaux.cnrs.fr

Z. Naturforsch. **61b,** 1527 – 1540 (2006); received July 3, 2006

High oxygen pressures are a fruitful tool for the stabilization of the highest formal oxidation states of transition metals (M^{n+}) leading to the strongest chemical bonds; the improvement of the M^{n+}–O bond covalency induces different electronic phenomena. Among the physical characterizations applied to investigate such phenomena, ^{57}Fe and ^{119}Sn Mössbauer spectra are evaluated for studying unusual electronic configurations, orbital ordering, charge disproportionation and insulator-metal transitions in the perovskites series of ^{57}Fe doped *RE*NiO_3 nickelates (*RE* = rare earths, Y and Tl) and ^{119}Sn doped *AE*FeO_3 ferrates (*AE* = Ca, Sr).

Key words: Oxygen Pressure, High Oxidation States, Mössbauer Spectroscopy, Electronic Configuration, Orbital Ordering, Charge Disproportionation, Insulator to Metal Transition

Introduction

The synthesis of novel materials has been an important challenge during the second part of the XXth century with two main motivations:

(i) to improve the knowledge of the correlations between composition – structure – chemical bonding and the resulting physico-chemical properties;
(ii) to support the technological development by proposing novel materials with specific properties.

In a first approach the synthesis of novel materials is closely dependent on three main factors: the reactivity of the precursors, the involved process (reaction in solid state, hydrothermal or solvothermal reactions in a liquid phase, CVD deposition from the gas phase), and the thermodynamic parameters (temperature and pressure). All of these factors have been investigated during the early stages of Materials Chemistry.

During the last fifty years, the influence of the pressure parameter was investigated in Materials Chemistry and Materials Science with respect to the synthesis of specific materials: diamond for tooling applications [1], chromium dioxide for magnetic recording [2], and α-quartz for frequency devices [3]. In a first step, the synthesis of novel oxides has mainly attracted scientists in fundamental research (the discovery of high T_c superconductors being an example [4, 5]).

In order to open the field of novel oxides, high oxygen pressures were applied with three main objectives:

– to study metal-oxygen phase diagrams [6, 7];
– to expand phase diagrams (in particular to include thermally unstable oxides [8, 9]);
– to stabilize unusual oxidation states of transition metals [10].

Three main routes were developed for producing oxygen pressures:

– the direct [11] or indirect oxygen gas compression [12];
– the use of oxidizing liquid media [13, 14];
– the development of oxidizing conditions in the solid phase using the thermal decomposition of different oxygen sources ($KClO_3$, $KClO_4$ ...) [13, 15].

In addition to oxygen pressures, other oxidizing processes have been investigated: electrochemical oxida-

Table 1. Some high oxidation states of the first row transition metals (Fe, Co, Ni, Cu).

Metal	Formal Oxidation State	Compound
Fe	+4	$CaFeO_3$ [20]
		$SrFeO_3$ [21]
		$A_{0.50}La_{1.5}Li_{0.50}Fe_{0.50}O_4$ (A = Ca, Sr, Ba) [22]
		$SrLaM_{0.50}Fe_{0.50}O_4$ (M = Mg, Zn) [23]
	+5	La_2LiFeO_6 [24]
Co	+3	$RECoO_3$ (RE = rare-earth) [25]
		$SrRECoO_4$ (RE = rare-earth) [26]
		$La_2Li_{0.50}Co_{0.50}O_4$ [27]
	+4	$Sr_{0.50}La_{1.5}Li_{0.50}Co_{0.50}O_4$ [28]
Ni	+3	$RENiO_3$ (RE = rare-earth) [29]
		$SrRENiO_4$ (RE = rare-earth) [30]
Cu	+3	$LaCuO_3$ [31]
		$La_2Li_{0.50}Cu_{0.50}O_4$ [31 – 34]
		$SrLaCuO_4$ [35]

tion [16], oxidation through ozonization [17], oxidizing fluxes using hydroxides [18, 19].

The Stabilization of High Oxidation States of Transition Metals

The stabilization of a specific oxidation state depends on the thermodynamic conditions used for preparing the expected solid. In the case of oxides, the stabilization of an oxidation state M^{n+} is correlated to the oxygen pressure value (pO_2):

$$A_{(\text{solid})} + M_{(\text{solid})} + m/2\ O_2 \rightarrow AM^{n+}O_m,$$
$$\Delta G = \Delta G^0 - m/2RT \cdot \log(pO_2).$$

Consequently, the increase of oxygen pressure induces a reduction of the ΔG value and allows the synthesis of the stoichiometric oxide with the formal oxidation state (n+).

Table 1 gives some formal high oxidation states of the first row transition metals stabilized under oxygen pressures in specific structures derived from the perovskite type. The stabilization of such oxidation states depends not only on the applied oxygen pressure but also on several chemical and structural parameters.

Transition metal oxides with high oxidation states are "acidic" and the metal-oxygen bonds are strongly covalent. Chemists know how to stabilize these oxides by interaction with a strongly basic metal oxide. The ionic bond created in this way allows the oxygen atoms to involve mainly their $2p_\sigma$ orbitals in the σ bonds with the transition metal. By this method, Demazeau *et al.* synthesized the first $LaLi_{0.5}Fe_{0.5}O_3$ perovskite with Fe^{5+} [24] and (La $AE)_2Li_{0.5}M_{0.5}O_4$ (where AE = Ca, Sr, Ba; $M = 3d$ transition metal) with a K_2NiF_4-type structure with M = high spin Fe^{4+} [22]. In this last Fe^{4+}oxide, the Li/Fe ordering within the the (001) planes allows the equatorial oxygen atoms to use only their $2p_\sigma$ orbitals to form four strong σ(Fe–O) bonds. This effect destabilizes the $d_{x^2-y^2}$ orbital which then is electron deficient.

In addition to the competitive chemical bonds, the electronic configurations of the M^{n+} cation must be adapted to the local symmetry of the (MO_6) polyhedra [36]. For example, the stabilization of Fe^{5+} ions, with the isotropic electronic configuration d^3 (*i. e.* $t_{2g}^3 e_g^0$), is appropriate for local O_h symmetry and consequently the $LaLi_{0.50}Fe_{0.50}O_3$ perovskite structure was selected. By contrast, the stabilization of the transition metal Jahn-Teller (JT) high spin Fe^{4+} ions with a single electron in a degenerate ground state ($d^4 \Rightarrow t_{2g}^3 e_g^1$) leads to D_{4h} symmetry and the $Sr_{0.50}La_{1.50}Li_{0.50}Fe_{0.50}O_4$ oxide with the K_2NiF_4 structure was selected as a host structure. The ($Fe^{4+}O_6$) octahedron is strongly elongated as illustrated by a large c/a ratio of 3.46. This high value confirms a high spin configuration for Fe^{4+} ($d_{xz}^1 d_{yz}^1 d_{xy}^1 d_{z^2}^1 d_{x^2-y^2}^0$).

Consequently, the stabilization of a specific M^{n+} oxidation state depends on different factors:

(i) the oxygen pressure value (while the preparation of $LaLi_{0.5}Fe_{0.5}O_3$ required 5 GPa [24], the synthesis of the Fe^{4+} oxide ($Sr_{0.50}La_{1.50}Li_{0.50}Fe_{0.50}O_4$) needed only 200 MPa [22]);
(ii) the modification of the chemical bond and the local crystal field energy;
(iii) the local (MO_6) symmetry required by the electronic configuration.

This paper is focussed on the resulting electronic phenomena in oxides containing transition metals in the highest oxidation states. The identification and the characterization of such phenomena is of prime importance.

The Electronic Phenomena Associated with the Increase of a Formal Oxidation State

The increase of the formal oxidation state (n) of a transition metal (M^{n+}) leads to an important shrinking of the M^{n+}–O bond length. Table 2 gives an illustration of these trends for the iron oxides (from Fe^{2+} to

Table 2. Evolution of the Fe^{n+}-O distances *versus* the formal $n+$ value [$r(Fe^{n+})$ defined on the basis of $r(O^{2-}) = 1.40$ Å] [37].

Formal oxidation state	Compound	Fe^{n+}–O (Å)	$r(Fe^{n+})$ (Å)
+3	$LiFeO_2$	2.03	0.63
+4	$Sr_{0.50}La_{1.50}Li_{0.50}Fe_{0.50}O_4$	1.95_6	0.55_6
+5	La_2LiFeO_6	1.86	0.46

Fe^{5+} in order to keep the octahedral iron coordination constant). The strong decrease of the metal-oxygen bond length induces an increase of the covalency of the *M*–O bonds. Theoretical justification of this rule comes from calculations of $b^{ca} \sim r^{-n}$, which gave $n = 2.5-3$ for the M^{n+}–O bond length r [38, 39] (b^{ca} is a resonance integral describing the energy of a virtual charge transfer to the $M : d^{n+}$ orbitals from the near-neighbour $O : 2p(2s)$ orbitals) [40]. Thus, the remarkable change in covalency, induced by the increase of the formal oxidation state for a transition metal is able to modify the electronic properties of the corresponding oxides.

These properties can be classified in two main categories:

– the intra-atomic ones – the same 3*d* orbitals of the M^{n+} cation being involved;
– the inter-atomic ones – different M^{n+} cations or different atoms (M^{n+} and O^{2-}) being implied.

The intra-atomic electronic properties

Regarding intra-atomic electronic properties, the change of the electronic configuration modifies the crystal field splitting $(10Dq)$ and the spin pairing energy (P). Taking into account that in oxides containing a 3*d*-block transition-metal M^{n+}, the energies 10*D*q and *P* have the same order of magnitude; d^n configurations may be either high-spin $(P > 10Dq)$ or low-spin $(10Dq > P)$. The covalent mixing of $O^{2-} : 2p$ with $M^{n+} : 3d$ orbitals lowers the spin pairing energy *P* (nephelauxetic effect) and increases 10*D*q. Therefore, stronger covalent mixing stabilizes low-spin relative to high-spin configurations. This implies that the covalency of *M*–O bonds plays an important role in inducing the spin-state transitions.

The above phenomenon can be observed in particular for $Co^{3+} : d^6$ ions in oxygen lattices for which low-spin (LS) to high-spin (HS) transitions and a semiconductor-metal transition have been reported. It was suggested that for the Co^{3+} ions the crystal field energy 10*D*q is only slightly larger than the spin pairing energy $P = 3J_{ex}$ (were J_{ex} is the intra-atomic (Hund) exchange integral). Thus the ground state of the Co^{3+} ions is LS ($t_{2g}^6 e_g^0$, S = 0) and the excited state HS ($t_{2g}^4 e_g^2$, S = 2) is only 0.08 eV higher in energy [41 – 43]. An increase in temperature leads to the population of the HS states which is reflected in results of magnetic susceptibility measurements [44].

The electronic configuration of transition metal ions depends not only on the crystal field splitting and the intra-atomic spin pairing energy but also on the distortion of the anionic surrounding. Buffat *et al.* [36] have plotted the variation of the energy of the various electronic terms as a function of an axial distortion parameter (θ) equal to the ratio of the metal-ligand distance $(d_\parallel)$ along the fourfold axis, to that $(d_\perp)$ in the perpendicular plane $(\theta = d_\parallel / d_\perp)$.

In Fig. 1, reproducing the results for the D_{4h} symmetry of a d^8 configuration, we can see that the $^1A_{1g}$ term (S = 0) with the holes in the $d_{x^2-y^2}$ orbital corresponding to the LS diamagnetic state ($d^6_{xz,yz,xy} d^2_{z^2} d^0_{x^2-y^2}$ is favoured by (*i*) a strong crystal field *D*q value; (*ii*) a high covalency and a small value of the Racah parameter *B*, and (*iii*) a large elongation of the octahedron, square planar being the most appropriate coordination. This explains why Cu^{3+} or Au^{3+} formal oxidation states can easily be obtained in square planar coordination ($\theta \to \infty$) [36]. Six-coordinated Cu^{3+} has first been obtained under high oxygen pressure: in elongated octahedral oxygen coordination in the $La_2Li_{0.5}Cu_{0.5}O_4$ oxide with K_2NiF_4-type structure with a Cu^{3+} low-spin d^8 configuration ($d^6_{xz,yz,xy} d^2_{z^2} d^0_{x^2-y^2}$), or in roughly non-distorted octahedra leading to *d* electron delo-

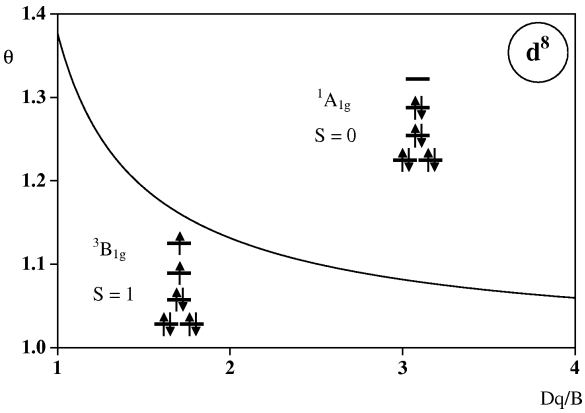

Fig. 1. Diagram showing the stabilized ground state regions for a d^8 configuration as a function of the octahedron elongation (θ) and of the crystal field (*D*q) and Racah (*B*) parameters.

calization like in metallic $LaCuO_3$ [31] where Cu^{3+} adopts the $t_{2g}^6\sigma^{*2}$ configuration.

The inter-atomic electronic properties

Regarding the inter-atomic electronic properties, three main phenomena can be encountered:

(i) a charge transfer ($d^n \rightarrow d^{n+1}\underline{L}$, where $\underline{L}$ represents a hole in the $2p$ orbital of a ligand) [45],
(ii) the charge disproportionation ($2M^{n+} \Leftrightarrow M^{(n+\varepsilon)+} + M^{(n-\varepsilon)+}$) [46],
(iii) the insulator → metal transition ($t_{2g}^n e_g^m \rightarrow t_{2g}^n \sigma^{*m}$) [47].

Several different parameters play a role in such electronic phenomena:

- The energy Δ, corresponding to the electronic transfer ($d^n \rightarrow d^{n+1}\underline{L}$), can – through the creation of holes at the anion sites – modify the general electronic properties of the corresponding oxides [48]. If the top of the $O^{2-}:2p^6$ bands lies in the gap U' between successive redox energies $M^{(n+1)+/n+}$ and $M^{n+/(n-1)+}$, the lower redox couple becomes pinned to the top of the O:$2p$ bands and the effective gap between the pinned redox couple ($O^{2-}:2p^6$) and the upper couple ($M^{(n+/(n-1)+}$) is referred to as a charge-transfer gap ($\Delta < U'$) [49].
- The on-site Coulomb energy U' separating successive redox couples $M^{n+}/M^{(n-1)+}$ is responsible for localizing electrons in single-valent compounds; the decrease of the metal-oxygen length suppresses U' and converts the localized electrons into itinerant electrons occupying an energy band width W. At the crossover from a localized to an itinerant electronic state ($U' \approx W$) disproportionation can take place [40].
- The band-width W in the itinerant-electron limit: The tight-binding band theory for itinerant electrons ignores U' to give a band-width $W \sim 2zb^{cac}$, were z is the number of the nearest neighbours. The improvement of the transfer integral b^{cac} *versus* the strength of the M^{n+}-O bond and the structural distortion (the M^{n+}–O–M^{n+} angle associated with the overlap of orbitals) can strongly influence the insulator to metal transition.

Usually, the electronic structure of 3*d*-transition-metal oxides is described by the Zaanen-Sawatzky-Allen (ZSA) scheme [49] in two regimes according to the relative magnitude of the charge-transfer energy Δ and the on-site Coulomb energy U' (Fig. 2).

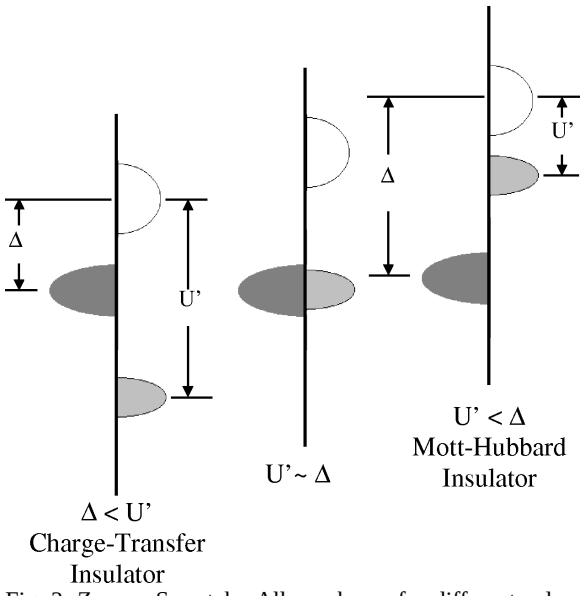

Fig. 2. Zaanen-Sawatzky-Allen scheme for different values of parameters Δ, W, U'.

In the *Mott-Hubbard regime*, the magnitude of the band gap is given by U', while in the *charge-transfer regime*, it is given by $\Delta(\Delta < U')$. With an increasing formal oxidation state of the 3*d*-metal, the Δ value systematically decreases. It is then expected that Δ may become very small. For compounds with unusually high valence states such as Fe^{4+}, Co^{4+}, Ni^{3+}, Cu^{3+}, Δ can be negative. These compounds have ground states which are dominated by the ligand hole character ($d^{n+1}\underline{L}$; $d^{n+2}\underline{L}^2 \ldots$) due to small or even negative Δ values [50]. The resulting properties of such systems are complex and not yet understood.

The characterization of the electronic properties (spin transition, disproportionation, insulator → metal transition …) is a challenge.

Physical Techniques for Investigating the Electronic Phenomena

Several physical techniques have been developed for investigating the electronic phenomena induced by the variation of the strength of the chemical bond through the increase of the formal oxidation state.

Unusual electronic configurations and spin transitions

It is known that *p-d* hybridization can change the order of the states in spin multiplets [51]. The perovskite

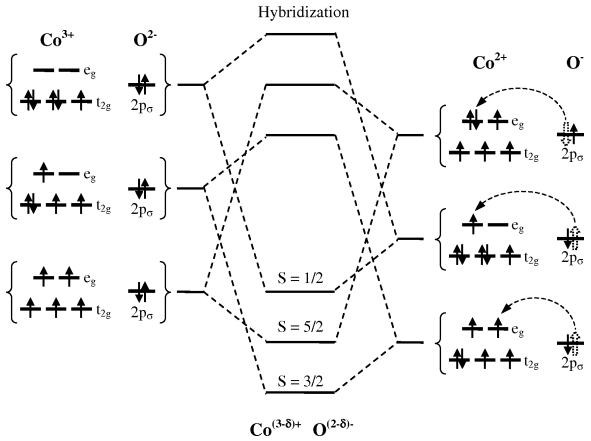

Fig. 3. A sheme of the formation of an intermediate spin state due to the relative stability of the $d^6\underline{L}$ states.

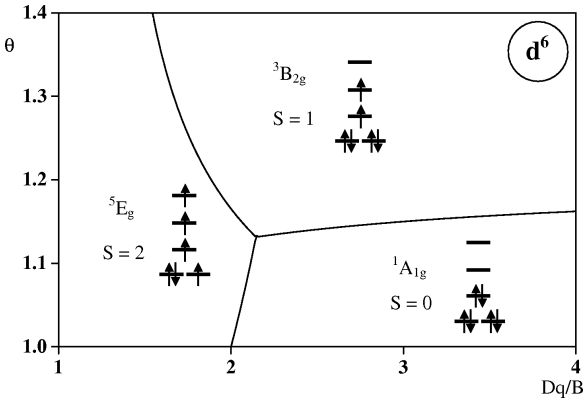

Fig. 4. Diagram showing the stabilized ground state regions for a d^6 configuration as a function of the octahedron elongation (θ) and of the crystal field (Dq) and Racah (B) parameters.

$SrCoO_3$ containing cobalt in the unusually high valence state of Co^{4+} provides a good example for such a behavior [52]. In a purely ionic picture, the ground state of the Co^{4+}: d^5 cation in the cubic field should be either high-spin ($S = 5/2$) or low-spin ($S = 1/2$). However, the situation may drastically change when a negative charge-transfer Δ value is allowed. In this case the extra hole is predominantly located on oxygen and the charge-transfer configuration $d^6\underline{L}$ becomes lower in energy than a d^5 one. Thus the ground state of $SrCoO_3$ is expanded in terms of the *d-p* hybridization of d^5 (22%), $d^6\underline{L}$ (67%) and $d^7\underline{L}^2$ (11%) configurations [53, 54].

If the $d^6\underline{L}$ configuration is dominant, then the ground state of the d^6 configuration would have the lowest energy. The intermediate $^4T_{1g}$ ($t_{2g}^4 e_g^1$) spin state hybridizes with a $d^6\underline{L}$ state which has the high-spin configuration $t_{2g}^4 e_g^2$. This means that the $S = 3/2$ state may serve as an alternative ground state of the $Co^{3+}(O_6)^{-11}$ cluster rather than $Co^{4+}(O_6)^{-12}$, ensuring a high-spin local moment ($S = 2$) for Co^{3+}: d^6, in accordance with Hund's rule. An illustration of the formation of an intermediate-spin ground state is given in Fig. 3 where the relative stability of the ligand hole states determines the symmetry of the ground state. The intermediate-spin configuration can be visualized as high-spin Co^{3+}: d^6 ($S = 1$) with a hole antiferromagnetically coupled in a linear combination of oxygen $2p_\sigma$ orbitals which hybridize with the d electrons of e_g symmetry resulting in a total spin $S = 3/2$. A $S = 3/2$ ground state has been suggested from the interpretation of the Co2*p* XAS spectrum for $SrCoO_3$ [54].

Among the possible changes of the electronic configurations, the most investigated have been the transitions between the different electronic configurations of trivalent cobalt. In an oxygen host structure containing Co^{3+}: d^6, the crystal field energy (Dq) which stabilizes the LS configuration ($S = 0$) is close to the exchange energy (J_{ex}) which favours the HS state ($S = 2$). Many studies have been carried out on the LS → HS electronic transition [55–57]. This transition is actually observed for the perovskites $RECoO_3$ and $RE_{1-x}AE_xCoO_3$ (RE = rare earth; AE = Ca, Sr, Ba), where the local symmetry at the Co^{3+} ions is practically cubic [58, 59].

According to the diagram in Fig. 4, for $Dq/B \approx 2$ an important axial distortion can stabilize the $^3B_{2g}(^3T_{2g})$ state with an intermediate electronic configuration: $d_{yz}^2 d_{zx}^2 d_{xy}^1 d_{z^2}^1 d_{x^2-y^2}^0$. In order to obtain $^3B_{2g}$ as the ground state, it would be necessary to have simultaneously a strong Dq/B and a high θ value. This has been proved by introducting Co^{3+} ions in the strongly elongated sites of K_2NiF_4-type oxides, (such as $La_2Li_{0.50}Cu_{(0.50-x)}Co_xO_4$) which allow for the first time the observation of a majority of intermediate spin Co^{3+} ions at high temperature [60].

The spin-transition can be initiated by different parameters: temperature (reducing the local crystal field energy due to thermal vibrations), and pressure (improving the local crystal field energy value).

Different physical techniques have been used for following such spin transitions: Photoelectron spectroscopy [61], magnetic measurements [62], resonant X-ray scattering and X-ray absorption spectroscopy

[63], infrared spectroscopy [64], high resolution photo emission spectroscopy [65] and electron spin resonance [66].

Charge ordering and disproportionation

According to the ZSA scheme (Fig. 2), in most of the 3*d* transition metal oxides with small or negative Δ values ($\Delta < U'$; $\Delta < W_{\sigma,\pi}$), the highest part of the oxygen 2*p* bands can overlap with the lowest part of the 3*d* upper Hubbard band, and some holes are transferred from 3*d* orbitals to the 2*p* orbitals in the ground state. Thus these compounds should be metallic, but actually many compounds with unusually high metal valences exist as insulators. The first claim for the nature of a gapped (insulating) state in the 3*d* transition metal oxides with $\Delta < 0$ was made by Mizokawa *et al.* [67]. Their conclusion was based on the configuration interaction approach [68] and on Hartree-Fock (HF) calculations on *d*-*p*-type structure models [69].

It was found that the gap can correspond to two types of charge ordered states: (*i*) a state with charge ordering at the oxygen sites (OCO) that is induced by charge disproportionation in the oxygen substructure: $d^n\underline{L} + d^n\underline{L} \rightarrow d^n + d^n\underline{L}^2$; (*ii*) a state with charge ordering at the transition metal (MCO), which is a consequence of the charge disproportionation in the metal substructure: $d^n + d^n \rightarrow d^{n-1} + d^{n+1}$ (while the oxygen sites are occupied by the same number of holes $\underline{L}$). HF calculations have shown that the OCO state has lower energy than the MCO state for small Δ values, while the MCO state becomes lower in energy at $\Delta < 0$ due to the structural distortion [67].

This phenomenon can be observed for $CaFeO_3$, which belongs to the negative-Δ regime ($\Delta \approx 0$, $\Delta_{\text{eff}} \approx -3$ eV [70], were Δ is defined with respect to the centre of gravity of each d^n and d^{n+1} configuration, whereas Δ_{eff} is defined with respect to the lowest multiplet level of each configuration. Mössbauer spectroscopy studies of $CaFeO_3$ at 4.2 K reveal the presence of two chemically distinct iron sites with different hyperfine fields present in equal proportions [71, 72]. This observation has led to the widely held view that charge disproportionation of the type 2 $Fe^{4+}(d^4) \rightarrow Fe^{3+}(d^5) + Fe^{5+}(d^3)$ occurs in $CaFeO_3$. Taking into account that the Δ_{eff} value is highly negative, the MCO state occurs even without the strong breathing-type distortion. The crystal structure of $CaFeO_3$ has been determined using synchrotron X-ray techniques [73]. It was shown that at low temperatures the structure belongs to the monoclinic space group $P2_1/n$, and contains two distinct Fe sites, which provides an evidence for charge disproportionation in the iron substructure.

Photoemission spectroscopy has been used to study oxygen-hole ordering and charge disproportionation in Fe^{4+} oxides with the perovskite structure [70, 74, 75]. It was found that the Fe^{4+} and Fe^{5+} formal oxidation states can be approximated as Fe^{3+} ions accompanied by single or double oxygen holes $d^5\underline{L}$ and $d^5\underline{L}^2$, respectively. In this view, the charge disproportionation may thus be presented as $2d^5\underline{L} \rightarrow d^5 + d^5\underline{L}^2$. The magnitude of the band gaps of the Fe^{4+} compounds is so small that a very minor structural distortion shifts the energy of the $\{d^5 + d^5\underline{L}^2\}$ state below that of the $\{d^5\underline{L} + d^5\underline{L}\}$ state, as the common background for the itinerant electron character of the cubic-perovskite (which has 180° Fe-O-Fe bonds) and the charge disproportionation in the distorted perovskite $CaFeO_3$ with Fe-O-Fe bond angles reduced to 150–160° [73]. Where the Fe(e_g)–O($2p_\sigma$)–Fe(e_g) interactions are stronger, as appears to be the case for $SrFeO_3$, the quarter-filled e_g orbitals become transformed into a narrow σ^* band of itinerant electrons, whithout disproportionation.

The above argument can also be applied to the electronic structure of Ni^{3+} compounds, namely, *RE*NiO_3 perovskites. The Δ_{eff} value of Ni^{3+} oxides is expected to be in the range 0–1 eV. In this case, the d^7 and $d^8\underline{L}$ states are nearly degenerate and strongly hybridized, leading to the formation of a split-off state as the ground state. Neutron diffraction has underlined the existence of two different nickel sites, $Ni^{(3-\alpha)}$ and $Ni^{(3+\alpha)}$, resulting from the Ni^{3+} disproportionation for the smallest rare earths (Ho → Lu) in the perovskite series *RE*NiO_3 [76, 77].

Insulator-metal transition

Insulator → metal transitions have been investigated by different physical techniques: electrical measurements [78], X-ray absorption spectroscopy (in the case of the nickelates *RE*NiO_3 [79]), differential scanning calorimetry measurements (in particular for *RE*NiO_3 single crystals) [15], high resolution synchrotron X-ray diffraction (as for $BaVS_3$ [80]).

The Potential of Mössbauer Spectroscopy for Studying Electronic Phenomena

The purpose of this paper is to evaluate the potential of Mössbauer spectroscopy, as a local physical technique, for characterizing electronic phenomena such as disproportionation and insulator-metal transition.

The physical characterizations can be classified in two main categories:

– those involving long range ordering;
– those identifying the local environment.

In Mössbauer spectroscopy three alternative situations are to be considered.

– The M^{n+} cation is a Mössbauer isotope as for example ^{57}Fe. In such a case the disproportionation of high spin Fe^{4+} was observed in the perovskite $CaFeO_3$ [71, 72].
– The M^{n+} cation is not a Mössbauer nucleus and consequently it is necessary to dope the oxide matrix by a Mössbauer isotope such as ^{57}Fe [81] or ^{119}Sn [82].
– The M^{n+} cation is a Mössbauer nucleus but a doping with another diamagnetic Mössbauer isotope can allow, in addition, to evaluate the transferred magnetic fields in the magnetically ordered temperature regime. As an example the $^{119}Sn^{4+}$ doping of the $CaFeO_3$ and $SrFeO_3$ perovskites has underlined the role of the steric effects of Sn^{4+} on the Fe^{3+} and Fe^{5+} distribution in the vicinity of the diamagnetic probe ^{119}Sn [83, 84].

Electronic states of the Fe(IV) ions in ferrates

^{57}Fe Mössbauer spectroscopy is one of the major method for studying the electronic microstructure of ferrates. Using this method, it was shown that $CaFeO_3$ and $SrFeO_3$ with perovskite-type structure have different electronic and magnetic properties [71, 72, 85 – 89].

The Mössbauer spectrum of $SrFeO_3$ consists of a single line above $T_n = 130$ K and a single magnetic hyperfine sextet below T_n. This behaviour is explained by the strong covalency of the Fe–O bonds leading to the formation of a σ^* band and to electron delocalization [90]. By contrast, the Mössbauer spectrum of $CaFeO_3$ below $T_n = 115$ K reveals two magnetic hyperfine sextets suggesting a charge disproportionation expressed formally as:

$$2Fe^{4+}(t_{2g}^3 e_g^1) \leftrightarrow Fe^{4-\varepsilon}(t_{2g}^3 e_g^{1+\varepsilon}) + Fe^{4+\varepsilon}(t_{2g}^3 e_g^{1-\varepsilon}),$$

where $\varepsilon = 0$ for $T > T_d$ (290 K) and ε increases with decreasing temperature (T_d = temperature of disproportionation). It was shown later that in the $Sr_{1-x}Ca_xFeO_3$ and $La_{1-x}AE_xFeO_3$ (*AE* = Ca, Sr) [71] solid solutions calcium substitution at any level (x) results in a disproportionation similar to that seen for $CaFeO_3$. A Mössbauer spectroscopic study of these systems revealed a delicate balance between the strength of the Fe–O–Fe interaction, the intra-atomic electron-electron correlation energy (U) and the electron-phonon interaction for the disproportionation reaction to occur [72]. For example, the disproportionation parameter (ε) was found experimentally to depend monotonically on the calcium content in each solid solution. However, the role of electron lattice interactions for the stability of the charge disproportionation still needs to be clarified.

To obtain a deeper insight into the electronic, magnetic and crystallographic structure of these compounds, diamagnetic probe Mössbauer spectroscopy of ^{119}Sn nuclei was applied [83, 90, 91]. This technique allows to obtain spectra of the Mössbauer diamagnetic cations, which are introduced in the structure of the compounds studied in very small quantities of 0.5-1 at. % (in order to prevent all possible perturbations of the structure). The use of diamagnetic atoms as Mössbauer probes appears to be most effective when studying magnetically ordered compounds. In this case, the inherent advantage of ^{119}Sn probes arises from the possibility to reveal the spin polarization of its electronic shell induced by the neighboring magnetic cations, which results in a Zeeman splitting in the ^{119}Sn Mössbauer spectra. Therefore, these magnetic spectra give to get direct information on the electronic configuration and the chemical bonding of the cationic surrounding of the diamagnetic Mössbauer probe, which generally cannot be obtained in the case of dia- or paramagnetic matrices.

Two main types of behavior have been observed in iron oxides $AEFeO_3$ (*AE* = Ca, Sr) doped with ^{119}Sn [84, 91, 92]: (*i*) the electron delocalization observed in stoichiometric $SrFeO_3$ can be locally impeded by Sn^{4+} doping, leading to Fe^{4+} disproportionation in the vicinity of Sn; (*ii*) the distribution of different iron cations Fe^{3+}/Fe^{5+} in the vicinity of Sn^{4+} is random for $SrFeO_3$ and essentially ordered for $CaFeO_3$ (with predominant presence of Fe^{4+} in the first cationic shell) underlining the importance of steric effects due to the size difference between Ca^{2+} and Sr^{2+}.

Mössbauer study of the nickelates $RENi_{0.98}Fe_{0.02}O_3$

The nickelates $RENiO_3$ (*RE* = Nd → Lu and Y) prepared first in 1971 by Demazeau *et al.* [29] have attracted considerable attention since this family exhibits

an insulator-metal (IM) transition at a temperature T_{IM} [7, 8] and a transition to an unusual long-range antiferromagnetic order below $T_n = T_{IM}$ (*RE* = Pr, Nd) or at $T_n < T_{IM}$ (*RE* = Sm → Lu, Y). These above physical phenomena are related to different factors: (*i*) the low-spin electronic configurations adopted by Ni^{3+} in an octahedral (NiO_6) site $(t_{2g}^6 e_g^1)$ due to the local Dq/B value; (*ii*) the strength of the Ni^{3+}–O bonds; (*iii*) the continuous increase of the structural distortion with the shrinking of the RE^{3+} ionic radius from La^{3+} to Lu^{3+} inducing a smaller Ni–O–Ni bond angle and, consequently, a decrease of the width $W_\sigma \sim (\cos\theta)$ of the σ^* band. The overlap of all these factors gives the opportunity to study electronic properties at the boundary between itinerant and localized π-bonding electrons [90].

Three main phenomena have been studied during the last twenty years:

- the orbital ordering characterizing the magnetic domains of $NdNiO_3$ and $SmNiO_3$ [93, 94];
- the disproportionation $2Ni^{3+} \rightarrow Ni^{(3+\varepsilon)+} + Ni^{(3-\varepsilon)+}$, recently observed through neutron diffraction studies for the smallest RE^{3+} (Ho → Lu) where the structural distortion improves the localization of the e_g^1 electron [76, 77].
- the insulator → metal transition (T_{IM}) is observed upon rising the temperatures for a constant composition *RE*NiO_3, the T_{IM} value increasing *versus* the structural distortion of the *RE*NiO_3 structure [78];

Mössbauer spectroscopy was recently employed for studying these phenomena into the *RE*NiO_3 nickelates.

Orbital ordering in magnetically ordered RE$Ni^{3+}O_3$ (RE = Nd, Sm) nickelates

A neutron diffraction study in the antiferromagnetic domain has underlined an unusual magnetic structure for the *RE*NiO_3 nickelates (*RE* = Pr, Nd, Sm, Eu) [93, 94]. In this structure each Ni^{3+} ion is coupled ferromagnetically to three nearest neighbours through the oxygen ions of the NiO_6 octahedron. In order to explain the antiferromagnetic properties an orbital ordering between $d^1_{x^2-y}$ and $d^1_{z^2}$ is proposed for the whole structure with two different sets of orbital surroundings for Ni(1) and Ni(2) for *RE*NiO_3 (*RE* = Pr, Nd, Sm).

Recently, we reported the hyperfine interaction parameters of ^{57}Fe atoms introduced as Mössbauer probes in $NdNiO_3$ and $SmNiO_3$ and discussed the magnetic structures in the light of the orbital ordering proposed by previous neutron diffraction studies [95, 96].

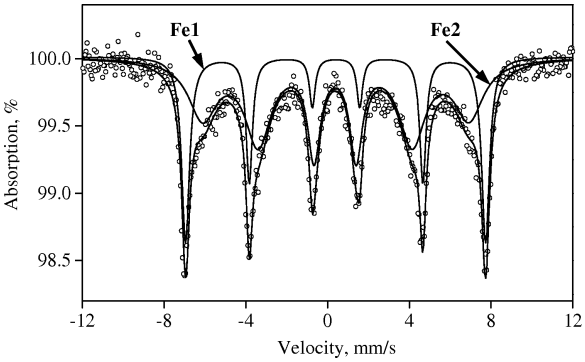

Fig. 5. ^{57}Fe Mössbauer spectrum of $NdNi_{0.98}Fe_{0.02}O_3$ at 60 K.

As an example, the ^{57}Fe Mössbauer spectrum at 4 K for $NdNi_{0.98}{}^{57}Fe_{0.02}O_3$ ($T_n = 150$ K) is presented in Fig. 5. This spectrum can be analyzed with two magnetic Zeeman sextets with approximately equal values for the chemical shifts ($\delta \approx 0.31$ mm/s) and similar quadrupole splittings. The magnetic hyperfine field values, H_1 and H_2, for the subspectra are considerably different $(H_1 \gg H_2)$. These features confirm that a statistically equal amount of probe atoms occupies two kinds of sites, Fe(1) and Fe(2), whose environments are chemically equivalent but magnetically different.

To explain this result the orbital ordering model proposed from neutron diffraction studies was used, with two cationic substructures Ni(1) and Ni(2) with respectively $(d^1_{x^2-y^2}, d^0_{z^2})$ and $(d^0_{x^2-y^2}, d^1_{z^2})$ electronic populations for the *e* orbitals. Such an orbital ordering leads to two different magnetic interactions: AF (antiferromagnetic interactions between two half-filled orbitals) and frustrated F (ferromagnetic interactions between a half filled orbital and an empty one) (Fig. 6). From this schematic description of the orbital ordering at the $^{57}Fe^{3+}$ cations and a consideration of the Kanamori-Goodenough rules (KG), two different magnetic e_g-p_σ-e_g superexchanges between Fe^{3+} and Ni^{3+} can be observed: interactions obeying the KG rules, and "frustrated" interactions for which the sign is in contradiction with the KG rules. Consequently Fe(1) substituting Ni(1) is characterized by two-dimensional magnetic interactions, and in contrast Fe(2) substituting Ni(2) is characterized by one-dimensional magnetic interactions. If the magnetic hyperfine field H_1 at the Fe(1) nuclei corresponds to bidimensional interac-

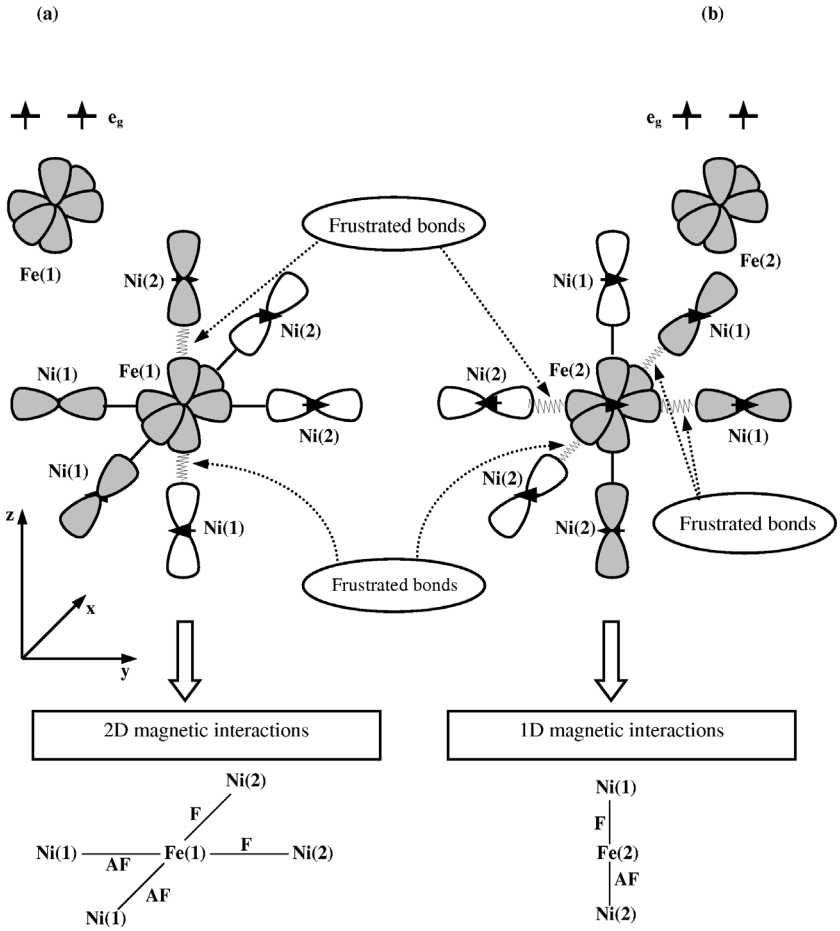

Fig. 6. A schematic representation of the orbital arrangement of the Fe(1) and Fe(2) probe atoms in the *RE*NiO_3 structure and the expected magnetic interactions.

tions, the smallest H_2 value at the Fe(2) nuclei is in agreement with one-dimensional interactions.

In conclusion, the Mössbauer spectroscopic study of $NdNiO_3$ and $SmNiO_3$ doped with ^{57}Fe probes confirms that orbital-ordering $(d^1_{x^2-y^2}, d^1_{z^2})$ leads to the observed two ^{57}Fe sites with different magnetic hyperfine field values.

Investigation of the disproportionation by Mössbauer spectroscopy

The structural distortion of the *RE*NiO_3 perovskites has a strong influence on their physical properties. This family undergoes two types of thermally induced transitions: an antiferromagnetic-paramagnetic transition (T_n), and an insulator-metal transition (T_{IM}). For the larger rare earths (Pr, Nd), $T_n = T_{IM}$, but when the structural distortion increases, $T_n \neq T_{IM}$ induces an intermediate insulator-paramagnetic domain $T_n < T < T_{IM}$. The increase of the structural distortion through the reduction of the Ni–O–Ni orbitals overlap leads to a decrease of the T_n values and an increase of the T_{IM} values from Sm to Lu.

After the detection – through neutron diffraction – of two different nickel sites in the *RE*NiO_3 lattice for *RE* : Ho → Lu [76, 77] – such nickelates were investigated using ^{57}Fe as a Mössbauer probe [97, 98].

In order to prevent strong modifications of the *RE*NiO_3 structure, a small doping rate (2 at. %) was used. Three different Ni^{3+} perovskites were first investigated: $LuNi_{0.98}{}^{57}Fe_{0.02}O_3$, $YNi_{0.98}{}^{57}Fe_{0.02}O_3$ and $TlNi_{0.98}{}^{57}Fe_{0.02}O_3$ (Tl being different from a rare earth element, the structural distortion of the $TlNiO_3$ structure is significantly different [99]). Fig. 7 gives the ^{57}Fe Mössbauer spectra at 300 K for these three perovskites.

These spectra can be described as a superposition of two quadrupole doublets. Such a deconvolution is in agreement with two different ^{57}Fe sites. The chemical

Table 3. ^{57}Fe Mössbauer parameters of $RE\mathrm{Ni}_{0.98}\mathrm{Fe}_{0.02}\mathrm{O}_3$ (RE = Y, Lu, Tl) at T = 300 K.

Compound	Site	δ, mm/s	Δ, mm/s	Γ, mm/s	S, %
$\mathrm{YNi}_{0.98}\mathrm{Fe}_{0.02}\mathrm{O}_3$	Fe(1)	0.32(1)	0.34(1)	0.30(1)	67(2)
	Fe(2)	0.18(1)	0.23(1)	0.31(1)	33(2)
$\mathrm{LuNi}_{0.98}\mathrm{Fe}_{0.02}\mathrm{O}_3$	Fe(1)	0.31(1)	0.38(1)	0.31(1)	66(2)
	Fe(2)	0.15(1)	0.21(1)	0.30(1)	34(2)
$\mathrm{TlNi}_{0.98}\mathrm{Fe}_{0.02}\mathrm{O}_3$	Fe(1)	0.36(1)	0.40(1)	0.30(1)	67(2)
	Fe(2)	0.23(1)	0.18(1)	0.31(1)	33(2)

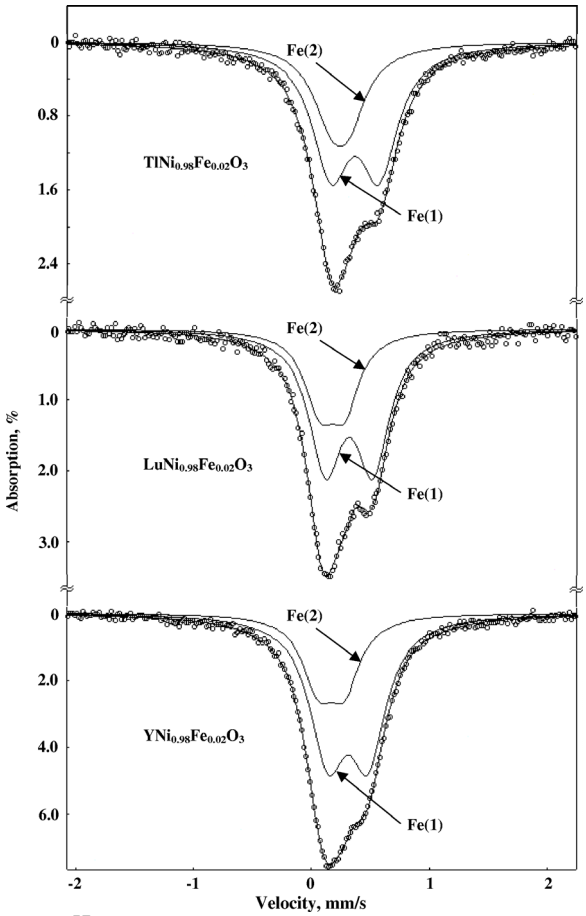

Fig. 7. ^{57}Fe Mössbauer spectrum of $RE\mathrm{Ni}_{0.98}\mathrm{Fe}_{0.02}\mathrm{O}_3$ (RE = Tl, Lu, Y) at 300 K.

shift values (δ_1, δ_2) for both quadrupole doublets are close to the δ values of Fe^{3+} (Table 3). The difference observed between the δ_1 and δ_2 values results from a difference of the corresponding Fe-O bond covalency in the ($Fe_{(1)}O_6$) and ($Fe_{(2)}O_6$) polyhedra. The existence of two different $^{57}Fe^{3+}$ sites with two Fe^{3+}–O bond strengths suggests two different nickel positions, each nickel atom being characterized by a different formal charge: $Ni^{(3-\varepsilon)+}$ and $Ni^{(3+\varepsilon)+}$. On the basis of the δ value correlated with the Fe–O bond strength, $Fe_{(1)}$ would be substituted for $Ni^{(3-\varepsilon)+}$ and $Fe_{(2)}$ for $Ni^{(3+\varepsilon)+}$ [97, 98].

In addition the quadrupole splitting values (Table 3), $\Delta_1 > \Delta_2$ in all cases are also in agreement with the neutron diffraction data underlining that the $[Ni^{(3-\varepsilon)+}O_6]$ polyhedra are more distorted than the $[Ni^{(3+\varepsilon)+}O_6]$ ones. The larger difference ($\Delta_1 - \Delta_2$) observed for the thallium perovskite confirms the strong distortion of such a structure due to the Tl^{3+} polarisation. Thus Mössbauer results confirm the results of a neutron diffraction study carried out by Alonso *et al.* [76, 77] and show that Mössbauer spectroscopy is useful for the investigation of disproportionation phenomena.

Characterization of the insulator-metal transition

In the pioneering works dedicated to study this class of oxides, the occurrence of thermally driven insulator → metal transitions has been related to the opening of a charge-transfer gap (Δ) between $O^{2-}:2p_\sigma$ and upper Hubbard $Ni^{3+}:3d_\sigma$ bands [9, 10] (Fig. 8). The width of the occupied $O^{2-}:2p_\sigma$ band is related to the $\vartheta_{ni-O-Ni}$ angle, which governs the $Ni:e_g$–$O:2p_\sigma$ overlap integral and, therefore, the covalent mixing parameter λ_σ entering the bandwidth W_σ [89]. As increasing the temperature enlarges the bandwidth, the Δ gap decreases, eventually going to zero, giving rise to a metallic state.

Recently, ^{57}Fe probe Mössbauer spectroscopy was used for following the insulator-metal transition *versus* temperature in the perovskites $NdNi_{0.98}{}^{57}Fe_{0.02}O_3$ and $LuNi_{0.98}{}^{57}Fe_{0.02}O_3$ [100, 101]. The main difference between the ^{57}Fe spectra of these nickelates was shown to be associated with the specificities of their local crystal structure.

The ^{57}Fe Mössbauer spectrum of a $NdNi_{0.98}{}^{57}Fe_{0.02}O_3$ sample measured at $T > T_{IM}$ can be described by one quadrupole doublet. Near the point $T \approx T_{IM}$ ($= T_n$), the monotonic change in $\delta(T)$ is violated by a decrease in the isomer shift ($\Delta\delta = 0.12$ mm/s) and a slight increase in the temperature coefficient $(\partial\delta/\partial T) = -9.2 \times 10^{-4}$ mm/s · K ($T < T_{IM}$) (Fig. 9). An explanation for the sharp jump of the temperature dependence $\delta(T)$ at $T = T_{IM}$ can be derived from specific features of the band structure of ^{57}Fe-doped $RE\mathrm{NiO}_3$ nickelates [101]. The energy diagram of Fig. 8 shows that for the metallic phase ($T > T_{IM}$) the 3*d* levels of the Fe^{3+} dopant cations

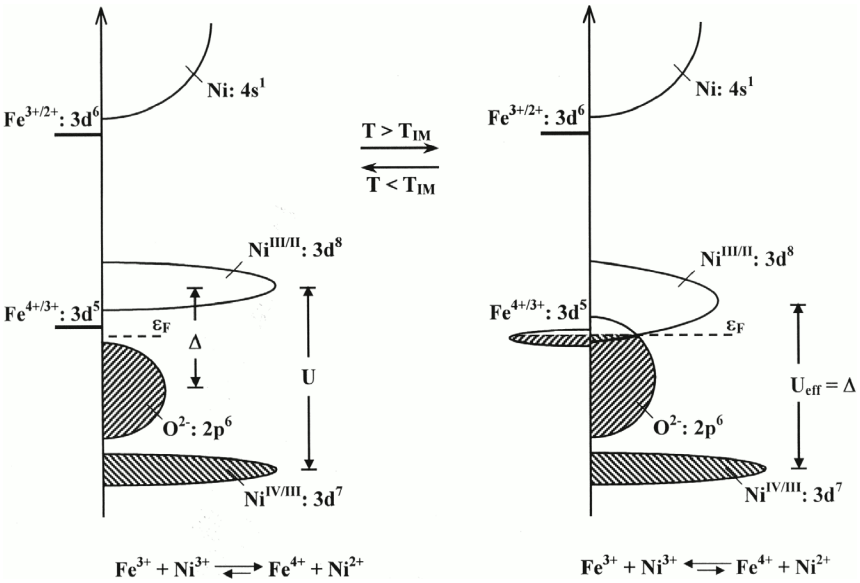

Fig. 8. Schematic energy diagram for the nickelate $NdNi_{0.98}Fe_{0.02}O_3$ on both sides of the point of the insulator-metal phase transition. The impurity levels of the Fe^{3+} cations are also shown.

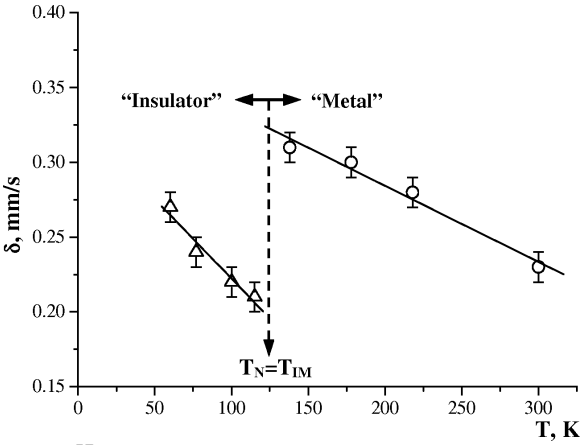

Fig. 9. ^{57}Fe chemical shift (δ) *vs.* temperature diagram for $NdNi_{0.98}Fe_{0.02}O_3$.

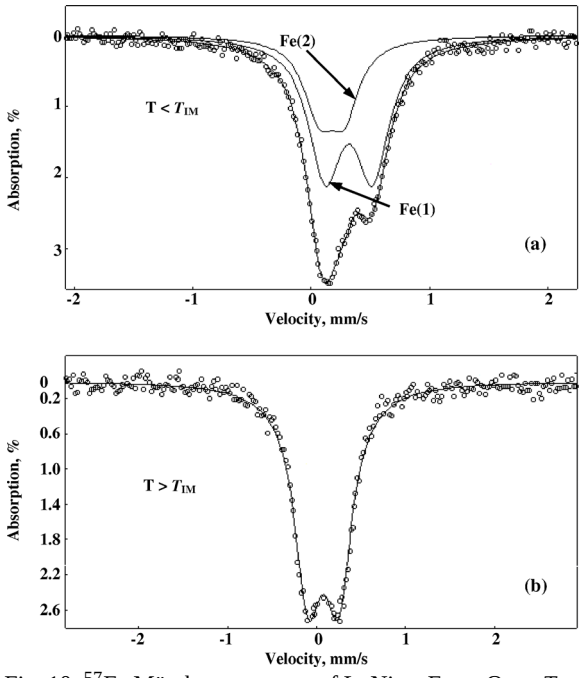

Fig. 10. ^{57}Fe Mössbauer spectra of $LuNi_{0.98}Fe_{0.02}O_3$ at $T < T_{IM}$ (a) and $T > T_{IM}$ (b).

penetrate into the valence band formed by an overlap of the $2p_\sigma$ bonding band of the O^{2-} anions and the vacant Hubbard e_g band of the Ni^{3+} cations. This leads to a broadening of the iron energy levels, which form a narrow band characterized by a high density of states and wave functions distributed outside the dopant cations.

Zunger *et al.* [102] showed that a similar delocalization of 3*d*-metal wave functions is responsible for a considerable decrease in the intra-atomic electron repulsion energy (U) compared to the corresponding values for free atoms. In turn, the decrease in U can result in a considerable redistribution of electrons between the valence 3*d* and 4*s* orbitals. In particular, it was shown for the Si : *M* system (*M* = Cu, Ni, Co, Fe, Mn, V, Ti) that, as a result of a decrease in U by several orders of magnitude, the transition-metal atoms *M* located in the silicon structure acquire the effective electronic configurations $3d^{m+1}4s^1$

or $3d^{m+2}4s^0$, which differ considerably from their electronic configurations in the free state ($3d^m4s^2$). Based on these results, we may assume that, for the $NdNi_{0.98}Fe_{0.02}O_3$ system, the transition to the metallic state ($T > T_{IM}$) will also be accompanied by a decrease in the intra-atomic energy U(Fe), which is favorable for a more efficient filling of the 3*d* orbitals of the Fe^{3+} impurity cations as compared to their state at $T < T_{IM}$. Since the 3*d* electrons are responsible for the shielding of *ns* electron density at the Fe^{3+} nuclei, the transition to temperatures $T > T_{IM}$ should be accompanied by a decrease in the isomeric shift (Fig. 8).

The ^{57}Fe spectra of $LuNi_{0.98}Fe_{0.02}O_3$ recorded in the insulator paramagnetic region, $T_n < T < T_{IM}$, consist of two quadrupole doublets (Fig. 10a) indicating that the ^{57}Fe dopant is located in two non-equivalent Fe(1) and Fe(2) crystallographic sites. This result is consistent with the observed monoclinic symmetry for the small rare-earth nickelates below T_{IM} [7, 16], which implies the existence of two types of alternating Ni(1)O_6 and Ni(2)O_6 octahedra. However, upon heating the $LuNi_{0.98}Fe_{0.02}O_3$ sample well above T_{IM}, the ^{57}Fe spectrum shows the abrupt convergence of the two Fe(1) and Fe(2) subspectra for the monoclinic-insulating phase, to one quadrupole doublet for the orthorhombic-metallic phase (Fig. 10b). This result suggests the formation of a unique state for iron probe atoms and therefore implies that the charge disproportionation in the NiO_6 subarray vanishes completely at the insulator → metal transition.

Thus, our findings show that the charge state and local environment of the probe ^{57}Fe atoms are very sensitive to a change in the electronic structure of the nickelates.

Conclusion

The stabilization under high oxygen pressures of the highest formal oxidation states of transition metals – in particular the 3*d* row – through the improvement of the strength of the M^{n+}–O bonds seems particularly important for inducing specific electronic phenomena.

Using ^{57}Fe as a probe, Mössbauer spectroscopy as a local physical characterization has been applied for studying electronic phenomena in $AEFeO_3$ (*AE* = Ca, Sr) and $RENiO_3$ perovskites (electronic configuration and oxidation state, orbital ordering, disproportionation, insulator to metal transition).

These recent results underline the potential of Mössbauer spectroscopy for investigating the electronic phenomena induced by the strengthening of chemical bonds in oxides.

Acknowledgements

The authors would like to acknowledge financial support by the Russian Foundation for Basic Research – CNRS (Ref. Nr. 05-03-22003), the French Research Agency CNRS (Department of Chemistry – PICS 3200) and the French Ministry for Foreign Affairs for supporting a thesis in co-tutelle between University Bordeaux 1 "Sciences and Technology" and University Lomonosov Moscow (A.B.). We also thank INTAS (Ref. Nr. 03-55-2453) for supporting A.B.

[1] P. Bernier, S. Lefrant, "Le Carbone dans tous ses Etats" Chap. 13, "Diamant et Matériaux Dérivés" G. Demazeau, Gordon-Breach Science Publishers (1997).
[2] D. K. Agrawal, A. K. Biswas, C. N. R. Rao, E. C. Subbarao, Mat. Res. Bull. **13**, 1135 (1978).
[3] F. Lafon, G. Demazeau, Matériaux et Techniques **3 – 4**, 11 (1997); **5 – 6**, 17 (1977).
[4] J. G. Bednorz, K. A. Müller, Z. Phys. B.: Condens. Matter **64**, 189 (1986).
[5] Y. Tokura, Physica C: Superconductivity **185 – 189**, 174 (1991).
[6] W. B. White, R. Roy, Ceramic Bull. **42**, 203 (1963).
[7] R. Roy, Colloque International CNRS Bordeaux (France), 1065 (1965).
[8] A. W. Sleight, Inorg. Chem. **8**, 1969 (1967).
[9] Th. Plante, G. Demazeau, M. Pouchard, P. Hagenmuller, Bull. Soc. Chim. **12**, 202 (1974).
[10] G. Demazeau, D. Y. Jung, Eur. J. Solid State Inorg. Chem. **32**, 383 (1995).
[11] G. Demazeau, Thèse Docteur és-Sciences Physiques, Université Bordeaux 1 (1973) N° 419.
[12] S. Kume, F. Kanamaru, Y. Shibasaki, M. Koizumi, K. Yasunami, T. Fukuda, Rev. Sci. Instrum. **42**, 1856 (1971).
[13] J. B. Mac-Chesney, H. J. Williams, R. C. Sherwood, J. F. Potter, J. Chem. Phys. **44**, 596 (1966).
[14] G. Demazeau, P. Maestro, Th. Plante, M. Pouchard, P. Hagenmuller, in B. Vodar and Ph. Marteau (eds): High Pressure Sciences and Technology **1**, 572 (1980).
[15] J. A. Alonso, M. J. Martinez-Lope, M. T. Casais, A. Munoz, A. Largeteau, G. Demazeau, MRS Spring Meeting (San Francisco, March 28 – 30, 2005) – Symposium Y "Solvothermal Synthesis of Materials" Proceedings **872E**, Y3.4-1 (2005).
[16] V. Pralong, V. Caignaert, S. Hebert, C. Marinescu, B. Raveau, A. Maignan, Solid State Ionics **177**, 815 (2006).

[17] W. Hesse, M. Jansen, W. Schnick, Prog. Solid State Chem. **19**, 47 (1989).
[18] R. G. Doisneau, B. Tremillon, J. Chim. Phys. **71**, 1445 (1974).
[19] C. N. R. Rao, J. Gopalakrishnan, New Directions in Solid State Chemistry Cambridge, University-Press (1997).
[20] F. Kanamaru, H. Miyamoto, Y. Mimura, M. Koizumi, M. Shimada, S. Kume, S. Shin, Mater. Res. Bull. **5**, 257 (1970).
[21] J. Mac-Chesney, R. C. Sherwod, J. F. Potter, J. Chem. Phys. **43(6)**, 1507 (1965).
[22] G. Demazeau, M. Pouchard, N. Chevreau, M. Thomas, F. Menil, P. Hagenmuller, Mater Res. Bull. **16**, 689 (1981).
[23] L. M. Zhu, G. Demazeau, L. Fournès, M. Pouchard, P. Hagenmuller, C. R. Acad. Sci. Serie II **304 (12)**, 633 (1987).
[24] B. Buffat, G. Demazeau, M. Pouchard, L. Fournès, J. M. Dance, P. Hagenmuller, C. R. Acad. Sci. Serie II **292**, 509 (1981).
[25] G. Demazeau, M. Pouchard, P. Hagenmuller, J. Solid State Chem. **9**, 202 (1976).
[26] G. Demazeau, Ph. Courbin, I. G. Main, G. Le Flem, C. R. Acad. Sci. Serie II **283**, 61 (1976).
[27] G. Demazeau, M. Pouchard, J. F. Colombet, J. C. Grenier, M. Thomas, L. Fournes, J. L. Soubeyroux, P. Hagenmuller, C. R. Acad. Sci. **289**, 231 (1979).
[28] B. Buffat, G. Demazeau, M. Pouchard, J. M. Dance, P. Hagenmuller, J. Solid State Chem. **50**, 33 (1983).
[29] G. Demazeau, A. Marbeuf, M. Pouchard, P. Hagenmuller, J. Solid State Chem. **3**, 582 (1971).
[30] G. Demazeau, M. Pouchard, P. Hagenmuller, J. Solid State Chem. **18**, 159 (1976).
[31] G. Demazeau, C. Parent, M. Pouchard, P. Hagenmuller, Mater. Res. Bull. **7**, 913 (1972).
[32] G. Villeneuve, T. Rojo, G. Demazeau, P. Hagenmuller, Mater. Res. Bull. **23**, 1787 (1988).
[33] A. Bianconi, J. Budnick, G. Demazeau, A. M. Flanck, A. Fontaine, P. Lagarde, J. Jegoudez, A. Revcolevski, A. Marcelli, M. Verdaguer, Physica C. **153 – 155**, 117 (1988).
[34] J. H. Choy, D. K. Kim, S. H. Hwang, G. Demazeau, J. Phys. Chem. **98**, 6258 (1994).
[35] J. B. Goodenough, G. Demazeau, M. Pouchard, P. Hagenmuller, J. Solid State Chem. **8**, 109 (1973).
[36] B. Buffat, G. Demazeau, M. Pouchard, P. Hagenmuller, Proc. Indian. Acad. Sci. (Chem. Sci.) **93**, 313 (1984).
[37] R. D. Shannon, C. T. Prewitt, J. Inorg. Nucl. Chem. **32**, 1247 (1970).
[38] K. N. Shrivastava, V. Jaccarino, Phys. Rev. B. **13**, 299 (1976).
[39] D. W. Smith, J. Chem. Phys. **50**, 2784 (1969).
[40] J. B. Goodenough, Magnetism and the Chemical Bond – New York: Wiley-Interscience (1963).
[41] G. Demazeau, S. H. Byeon, J. M. Dance, J. H. Choy, M. Pouchard, P. Hagenmuller, Eur. J. Solid State Inorg. Chem. **29**, 283 (1992).
[42] S. Yamaguchi, Y. Okimoto, H. Taniguchi, Y. Tokura, Phys. Rev. **B 53**, R 2926 (1996).
[43] M. Itoh, I. Natori, J. Magn. Magn. Mater. **140 – 144**, 2145 (1995).
[44] G. Demazeau, M. Pouchard, P. Hagenmuller, J. Solid State Chem. **9**, 202 (1974).
[45] G. van der Laan, J. Zaanen, G. A. Sawatzky, R. Karnatak, J. M. Esteva, Solid State Commun. **56**, 673 (1985).
[46] K. Kazushita, S. Morimoto, S. Nasu, Physica B **329 – 333**, 736 (2003).
[47] J. Z. Zhou, J. B. Goodenough, B. Dabrowski, P. W. Klamut, Z. Bukowski, Phys. Rev. B **61**, 4401 (2000).
[48] I. Solovyev, N. Hamada, K. Tarakura, Phys. Rev. B **53**, 7158 (1996).
[49] J. Zaanen, G. A. Sawatzky, J. W. Allen, Phys. Rev. Lett. **55**, 418 (1985).
[50] A. E. Bocquet, A. Fujimori, T. Mizokawa, T. Saitoh, H. Namatame, S. Suga, N. Kimizuka, Y. Takeda, M. Takano, Phys. Rev. B **45**, 1561 (1992).
[51] M. A. Korotin, S. Yu Ezhov, I. V. Solovyev, V. I. Anisimov, D. I. Khomshii, G. A. Sawatzky, Phys. Rev. B **54**, 5309 (1996).
[52] C. Zobel, M. Kriener, D. Bruns, J. Baier, M. Grüningen, T. Lorenz, F. Reutler, A. Revcolevski, Phys. Rev. B **66**, 020402(R) (2002).
[53] M. Abbate, G. Zampieri, J. Okamoto, A. Fujimori, S. Kawasaki, M. Takano, Phys. Rev. B **65**, 165120 (2002).
[54] R. H. Potze, G. A. Sawatzky, M. Abbate, Phys. Rev. B **51**, 11501 (1995).
[55] W. C. Koehler, E. O. Wollan, J. Phys. Chem. Solids **2**, 100 (1957).
[56] J. B. Goodenough, J. Phys. Chem. Solids **6**, 287 (1958).
[57] R. R. Heikes, R. C. Miller, R. Mazelsky, Physica **30**, 1600 (1964).
[58] M. A. Senaris-Rodriguez, J. B. Goodenough, J. Solid State Chem. **118**, 323 (1995).
[59] J. Wu, C. Leighton, Phys. Rev. B **67**, 174408 (2003).
[60] B. Buffat, G. Demazeau, M. Pouchard, P. Hagenmuller, Mater. Res. Bull. **18**, 1153 (1983).
[61] S. Vasudevan, H. N. Vasan, C. N. R. Rao, Chem. Phys. Lett. **65**, 444 (1979).
[62] G. Demazeau, S. H. Byeon, J. H. Choy, P. Hagenmuller, Z. Anorg. Allg. Chem. **610**, 91 (1992).
[63] G. Maris, Y. Ren, V. Volotchaev, C. Zobel, T. Lorenz, T. T. M. Palstra, Phys. Rev. B **67**, 224423 (2003).
[64] S. Yamaguchi, Y. Okimoto, Y. Tokura, Phys. Rev. B **55**, R8666 (1997).

[65] T. Saitoh, Y. Yamashita, N. Todoroki, T. Kyômen, M. Itoh, M. Higashiguchi, M. Nakatake, K. Shimada, J. Electron Spectroscopy Related Phenom. **144 – 147**, 893 (2005).
[66] S. Noguchi, S. Kawamata, K. Okuda, Phys. Rev. B **66**, 094404 (2002).
[67] T. Mizokawa, D. I. Khomskii, G. A. Sawatzky, Phys. Rev. B **61**, 11263 (2000).
[68] M. Abbate, H. Pen, M. T. Czyzyk, F. M. F. de Groot, J. C. Fuggle, Y. J. Ma, C. T. Chen, F. Sette, A. Fujimori, Y. Ueda, K. Kosuge, J. Electron Spectroscopy Related Phenom. **62**, 185 (1993).
[69] T. Mizokawa, A. Fujimori, Phys. Rev. B **51**, 12880 (1995).
[70] S. Fagot, P. Foury-Leylekian, S. Ravy, J. P. Pouget, M. Anne, G. Popov, M. V. Lobanov, M. Greenblatt, Solid State Sci. **7**, 718 (2005).
[71] M. Takano, Y. Takeda, Bull. Inst. Chem. Res. Kyoto Univ. **61**, 406 (1984).
[72] M. Takano, S. Nasu, T. Abe, K. Yamamoto, S. Endo, Y. Takeda, J. B. Goodenough, Phys. Rev. Lett. **67**, 3267 (1991).
[73] P. M. Woodward, D. E. Cox, E. Moshopoulou, A. W. Sleight, S. Morimoto, Phys. Rev. B **62**, 844 (2000).
[74] J. Matsuno, T. Mizokawa, A. Fujimori, K. Mamiya, Y. Takeda, S. Kawasaki, M. Takano, Phys. Rev. B **60**, 4605 (1999).
[75] J. Matsuno, T. Mizokawa, A. Fujimori, Y. Takeda, S. Kawasaki, M. Takano, Phys. Rev. B **66**, 193103 (2002).
[76] J. A. Alonso, J. L. Garcia-Munoz, M. T. Fernandez-Diaz, M. A. G. Aranda, M. J. Martinez-Lope, M. T. Casais, Phys. Rev. Letters **82**, 3871 (1999).
[77] J. A. Alonso, M. J. Martinez-Lope, M. T. Casais, J. L. Garcia-Munoz, M. T. Fernandez-Diaz, Phys. Rev. B **61**, 1756 (2000).
[78] J. B. Torrance, P. Lacorre, A. I. Nazzal, E. J. Ansaldo, Ch. Niedermayer, Phys. Rev. B **45**, 8209 (1992).
[79] M. Medarde, A. Fontaine, J. L. Garcia-Munoz, J. Rodriguez-Carvajal, M. de Santis, M. Sacchi, G. Rossi, P. Lacorre, Phys. Rev. B **46**, 14975 (1992).
[80] S. Fagot, P. Foury-Leylekian, S. Ravy, J. P. Pouget, H. Berger, Phys. Rev. Lett. **90**, 196401 (2003).
[81] I. A. Presniakov, G. Demazeau, A. V. Baranov, A. V. Sobolev, K. V. Pokholok, Phys. Rev. B **71**, 054409 (2005).
[82] G. Demazeau, M. Pouchard, P. Hagenmuller, P. B. Fabritchnyi, L. P. Fefilatiev, A. M. Babechkin, Mater. Res. Bull. **19**, 1337 (1984).
[83] G. Demazeau, P. Fabritchnyi, L. Fournès, S. Darracq, I. Presniakov, K. Pokholok, V. Gorkov, J. Etourneau, J. Mater. Chem. **5**, 553 (1995).
[84] G. Demazeau, P. Fabritchnyi, L. Fournès, S. Darracq, I. Presniakov, K. Pokholok, V. Gorkov, J. Etourneau, Zh. Neorgan. Khim. **40**, 616 (1995).
[85] J. B. Mac Chesney, R. C. Sherwood, J. F. Potter, J. Chem. Phys. **43**, 1907 (1963).
[86] F. Kanamaru, H. Miyamoto, Y. Miura, M. Koizumi, M. Shimada, S. Kume, Mater. Res. Bull. **5**, 257 (1970).
[87] Y. Takeda, S. Naka, M. Takano, T. Shinjo, T. Takada, M. Shimada, Mater. Res. Bull. **13**, 61 (1978).
[88] J. B. Mac Chesney, H. J. Williams, R. C. Sherwood, J. F. Potter, Mater. Res. Bull. **1**, 113 (1966).
[89] P. K. Gallagher, J. B. Mac Chesney, D. N. E. Buchanan, J. Chem. Phys. **45**, 2466 (1966).
[90] J. B. Goodenough, Rep. Prog. Phys. **67**, 1915 (2004).
[91] S. Darracq, G. Demazeau, P. B. Fabrichnyi, L. Fournes, I. A. Presniakov, K. V. Pokholok, V. P. Gorkov, Solid State Commun. **91**, 681 (1994).
[92] G. Demazeau, P. B. Fabrichnyi, L. Fournès, I. A. Presniakov, S. Darracq, V. P. Gorkov, K. V. Pokholok, J. Etourneau, Solid State Commun. **87**, 109 (1993).
[93] J. L. Garcia-Munoz, J. Rodriguez-Carvajal, J. B. Torrance, Phys. Rev. B **46**, 4414 (1992).
[94] J. L. Garcia-Munoz, J. Rodriguez-Carvajal, P. Lacorre, Phys. Rev. B **50**, 978 (1994).
[95] S. J. Kim, G. Demazeau, I. Presniakov, K. Pokholok, A. Baranov, A. Sobolev, D. Pankratov, N. Ovanesyan, Phys. Rev. B **66**, 014427 (2002).
[96] S. J. Kim, G. Demazeau, I. Presniakov, A. Baranov, A. Sobolev, D. Pankratov, K. Pokholok, O. Andreeva, N. Ovanesyan, Russ. J. Inorg. Chem. **48**, N^o 9, 1394 (2003).
[97] S. J. Kim, G. Demazeau, I. Presniakov, K. Pokholok, A. Sobolev, N. Ovanesyan, J. Amer. Chem. Soc. **123**, 8127 (2001).
[98] S. J. Kim, I. Presniakov, G. Demazeau, K. Pokholok, A. Baranov, A. Sobolev, D. Pankratov, N. Ovanesyan, J. Solid State Chem. **168**, 126 (2002).
[99] S. J. Kim, G. Demazeau, J. A. Alonso, J. H. Choy, J. Mater. Chem. **11**, 487 (2001).
[100] I. Presniakov, G. Demazeau, A. Baranov, A. Sobolev, K. Pokholok, Phys. Rev. B **71**, 054409 (2005).
[101] A. Baranov, I. Presniakov, G. Demazeau, A. Sobolev, N. Ovanesyan, D. Pankratov, K. Pokholok, S. Godovikov, Russ. J. Inorg. Chem. **50**, N^o 2, 246 (2005).
[102] A. Zunger, U. Lindefelt, Phys. Rev. B **27**, 1191 (1983).